

# Dsfer-Net: A Deep Supervision and Feature Retrieval Network for Bitemporal Change Detection Using Modern Hopfield Networks

Shizhen Chang, *Member, IEEE*, Michael Kopp, *Member, IEEE*, Pedram Ghamisi, *Senior Member, IEEE*

**Abstract**—Change detection, as an important application for high-resolution remote sensing images, aims to monitor and analyze changes in the land surface over time. With the rapid growth in the quantity of high-resolution remote sensing data and the complexity of texture features, a number of quantitative deep learning-based methods have been proposed. Although these methods outperform traditional change detection methods by extracting deep features and combining spatial-temporal information, reasonable explanations about how deep features work on improving the detection performance are still lacking. In our investigations, we find that modern Hopfield network layers achieve considerable performance in semantic understandings. In this paper, we propose a Deep Supervision and Feature Retrieval network (Dsfer-Net) for bitemporal change detection. Specifically, the highly representative deep features of bitemporal images are jointly extracted through a fully convolutional Siamese network. Based on the sequential geo-information of the bitemporal images, we then design a feature retrieval module to retrieve the difference feature and leverage discriminative information in a deeply supervised manner. We also note that the deeply supervised feature retrieval module gives explainable proofs about the semantic understandings of the proposed network in its deep layers. Finally, this end-to-end network achieves a novel framework by aggregating the retrieved features and feature pairs from different layers. Experiments conducted on three public datasets (LEVIR-CD, WHU-CD, and CDD) confirm the superiority of the proposed Dsfer-Net over other state-of-the-art methods. Code will be available online (<https://github.com/ShizhenChang/Dsfer-Net>).

**Index Terms**—Change detection, high-resolution optical remote sensing, modern Hopfield networks, Siamese convolutional network.

## I. INTRODUCTION

REMOTE sensing (RS) images-based change detection (CD) [1] is intended to identify and analyze land-cover variations from multi-temporal images whose geographical locations are correctly matched. This crucial image interpretation task has extensive applications in the analysis of spatiotemporal evolution of the Earth-surface, such as urban planning [2], disaster assessment [3], visual surveillance [4], and natural resources management [5], among others.

S. Chang and M. Kopp are with the Institute of Advanced Research in Artificial Intelligence, Landstraßer Hauptstraße 5, 1030 Vienna, Austria (e-mail: shizhen.chang@iarai.ac.at; michael.kopp@iarai.ac.at).

P. Ghamisi is the Institute of Advanced Research in Artificial Intelligence, Landstraßer Hauptstraße 5, 1030 Vienna, Austria, and also with the Helmholtz-Zentrum Dresden-Rossendorf (HZDR), Helmholtz Institute Freiberg for Resource Technology (HIF), Machine Learning Group, Chemnitz Str. 40, D-09599 Freiberg, Germany (e-mail: pedram.ghamisi@iarai.ac.at).

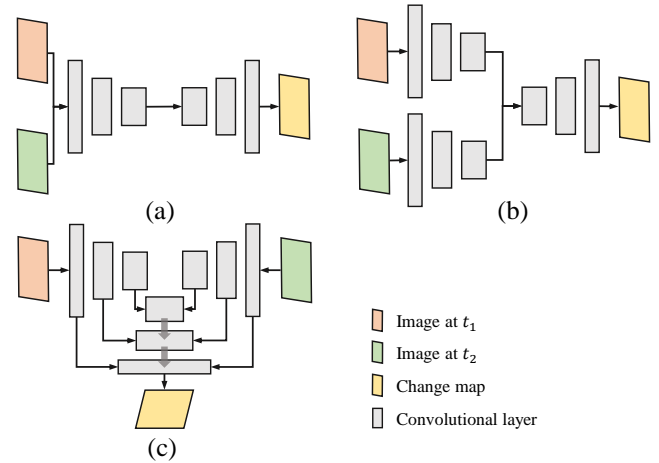


Fig. 1. Basic architectures of deep learning-based change detection methods. (a) Single-branch architecture. (b) and (c) Double-branch architectures.

In the past few decades, bitemporal change detection has received intensive attention, and myriad methods have been proposed, including traditional methods [6] and deep learning-based methods [7]. Before deep learning became widely used, change detection methods mainly focused on extracting explainable and handcrafted features through the use of statistical analysis [8], signal processing [9], or machine learning [10] methods. However, it is difficult to determine which method fits the best in practice, especially for relatively large datasets. Additionally, with the rapid development of high-resolution optical sensors (e.g., WorldView-3, GeoEys-1, QuickBird, and Gaofen-2) [11], the growing amount of accessible high-resolution remote sensing images has promoted a number of deep learning-based change detection methods with greater accuracy and more reliable geospatial understanding in complex data analysis.

As a powerful architecture of deep learning, convolutional neural networks (CNNs) have been used with increasing frequency since they have strong abilities to automatically extract hierarchical multilevel features and learn highly abstract semantic contexts that carry discriminative information about the changing areas. In contrast single-image processing tasks, designing an appropriate architecture to fuse the image pairs can improve the robustness of feature extraction and change diagnosis. As shown in Fig. 1, there are two main categories for feature fusion: single-branch architecture [12] and dual-branch architectures [13]. The single-branch architecture first

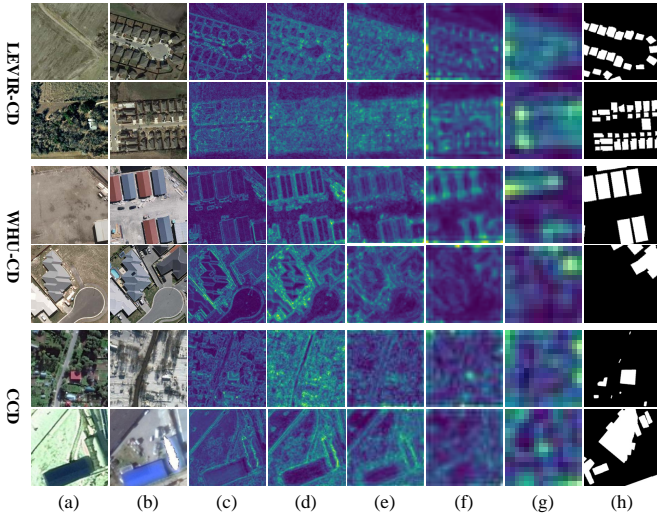


Fig. 2. Examples of the difference features from shallow to deep layers in a Siamese change detection network using VGG-16 as the backbone. (a) Images from  $t_1$ . (b) Images from  $t_2$ . (c) Features from the first stage. (d) Features from the second stage. (e) Features from the third stage. (f) Features from the fourth stage. (g) Features from the fifth stage. (h) Ground-truths.

fuses the two inputs by image concatenation or calculating the image difference, and feeds them into the network as a whole. It utilizes the early fusion (EF) strategy and then converts the fused image into high-level features, which only fuses partial information and can not fully consider individual information [14]. The dual-branch architecture is a late fusion strategy that first learns the single-temporal features, and then merges the learned features as the input of the decoder. Essentially, a Siamese neural network with shared weights has fewer parameters and faster convergence. Although the dual-branch architecture has better performance than the single-branch image-level fusion approach, it will inevitably be limited by the fact that the shallower layers cannot effectively learn useful features due to the vanishing gradient phenomena. Therefore, making a reasonable combination of the features from both deeper and less deep layers is more helpful to effectively identify the features of the original images that give rise to changes.

To solve the above-mentioned issues and accurately extract features, deeper and more complex CNN-based networks have been designed. We have known that features at shallow layers mainly contain the spatial structure of the image, such as texture, boundary, and colors, and those at deep layers contain more abstract content and representative semantic concepts [15]. Therefore, multi-scale fusion strategies (see Fig. 1(c) as a visual example) have been utilized to combine features from different layers. Many improved networks with enlarged receptive fields have been proposed, combined with other architecture components such as the generative adversarial network (GAN) [16], Long Short-Term Memory (LSTM) [17], and spatial and channel attention mechanisms [18]. However, the performance of change detection methods may not be improved by naively fusing the features learned by Siamese architecture with very deep layers, as a concomitant outcome is an explosion of parameters and computational memories.

As can be seen in Fig. 2, for a Siamese network using VGG-16 as the backbone, the features related to the changed area are best preserved in the mid-level layers, where the shallow layer retains abundant texture details but fails to exclude the information of the unchanged area. Furthermore, due to repeated pooling, the high-level features become too abstract and fuzzy for the network to accurately locate the change of interests. On the other hand, limited by the inherent architecture of CNNs, features from high levels are always directly related to the shallower layers of the corresponding branch, and the temporal information between the image pair is still not sufficiently explored.

In this paper, we propose a deep supervision and feature retrieval network for bitemporal change detection, abbreviated as Dsfer-Net. Inspired by modern Hopfield networks (MHNs) in deep learning, we design a deeply supervised feature retrieval (DSFR) module that applies dual Hopfield layers to aggregate space-time features from a sequential understanding and to track the changes in the image pairs between the two streams. Specifically, we insert deep supervision into the DSFR module to make sure that both semantic concepts and spatial structures of the changes in high-level features are well restored and retrieved. The decoder then decodes the concatenated feature pairs and connects them with the retrieved feature with a multi-scale fusion strategy to achieve accurate localization. Finally, a hybrid loss is used to minimize the errors of network propagation and feature retrieval for training purposes.

The main contributions of this article are summarized as follows:

- 1) We propose a novel change detection network that combines deep supervision and a retrieval concept for bitemporal remote sensing images. Here, we give further attempts to introduce Hopfield layers for change detection and explain the efficacy of deep feature retrieval and aggregation. The proposed network applies multi-scale fusion with a weighting strategy through a Siamese architecture to comprehensively capture the change of interests from shallow to deep layers.
- 2) To help high-level features preserve the changed information while generalizing semantic content, the deeply supervised feature retrieval module is designed for deep layers. It interprets the global context from a sequential understanding and can retrieve differences while the features are highly abstract. A hybrid loss is added to balance the error of the whole network and the Hopfield block.
- 3) Extensive experiments illustrate that the proposed Dsfer-Net has superior performance in maintaining the shape and preserving the boundaries of changed objects. In a comparison of different datasets, the proposed model shows significant superiority over other state-of-the-art models.

The rest of the article is structured as follows. Section II reviews related work. Section III introduces the proposed Dsfer-Net method. Section IV presents experiments and discusses the findings. Finally, the conclusions are outlined in Section V.

## II. RELATED WORK

### A. Deep Learning-Based CD Methods

According to various analyses of the purposes of change detection, deep learning-based CD methods can be categorized into three classes: pixel-based methods, object-based methods, and deep feature-based methods [19]. Pixel-based methods usually apply a deep neural network to transform the images into deep feature spaces, and then compare the features pixel by pixel to obtain the desired change output. For example, Zhang et al. [20] utilize a deep belief network (DBN) to capture the key information for discrimination. Then, the bi-temporal features are mapped into a 2-D polar domain to characterize the change information, and the changing map is obtained by adopting a supervised clustering algorithm. Du et al. [9] design a deep slow feature analysis module that first projects the input images into the deep feature space, then calculates the feature differences using the slow feature analysis metric, and obtains the change map. Chen et al. [21] utilize pre-trained VGG-16 architectures and attention mechanisms to extract features: the change map is ultimately derived by calculating the weighted double-margin contrast loss.

The main idea of object-based methods is to extract features by segmenting input images and then identify changes in the state of the segmented objects [14]. Ji et al. [22] present a hybrid CNN-based change detection framework where the buildings are viewed as objects and extracted through a mask R-CNN. Zhang et al. [23] proposed an end-to-end superpixel-enhanced CD network that adopts superpixel sampling networks to learn task-specific superpixels and uses the UNet-based Siamese network to exploit multi-level change clues. Liu et al. [24] propose an object-based change detection framework that utilizes CNN to extract features of image patches and combines different fusion strategies to discriminate the changes. We conclude that for both pixel-based and object-based change detection methods, deep learning modules such as DBN, LSTM, attention mechanism, and CNNs are utilized as a tool to transform raw images into high-level features, where the most discriminative information related to the change of interests is retained and the unchanged regions are suppressed.

Due to their excellent performance in feature extraction, CNN-based deep learning networks have been the most widely used for high-resolution remote sensing change detection tasks. To learn more reliable information from the available labeled data, end-to-end deep learning architectures, the fully convolutional neural networks (FCN), have been developed for deep feature-based change detection. In [25], Daudt et al. present three FCNs based on the UNet model: FC-EF, FC-Siam-conc, and FC-Siam-diff. The FC-EF method adopts an early fusion strategy that concatenates the image pairs as one input of the network; FC-Siam-conc and FC-Siam-diff are Siamese extensions of the FC-EF. The encoding layers of FC-Siam-conc and FC-Siam-diff are separated into two streams of equal structure with shared weights, as in a traditional Siamese network. The difference between these two models is that FC-Siam-conc concatenates the two skip connections

in the decoders, while FC-Siam-diff calculates the absolute value of feature differences and concatenates them with skip connections in the decoding stage. A similar architecture was simultaneously proposed in [26]. Later in [27], Daudt et al. modified the FC-EF architecture to use residual blocks with skip connections to improve the spatial accuracy of the result. Peng et al. [28] proposed an improved UNet++ network that first concatenates co-registered image pairs as an input, and then adopts the fusion strategy of multiple side outputs to combine change maps from different semantic levels.

Although these methods demonstrate good change detection capability, the spatial context information and the internal relationships from shallow to deep layers are still not fully taken into consideration. Thus, they are susceptible to pseudo-changes caused by noise, angle, shadow, and context. Therefore, many improved algorithms that consider features in both space and time dimensions have been proposed. Sun et al. [17] integrate the LSTM into the UNet architecture to use the convolutional LSTM as the core convolutional structure. This method combines convolution and recurrent structure and proves that RNNs are effective for capturing temporal relationships between images.

Recently, the attention mechanism has shown great potential in the image processing field: it can automatically return an enhanced feature based on the correlation among pixels in the feature itself. Peng et al. [12] present a difference-enhancement dense-attention convolutional neural network (DDCNN) that consists of several up-sampling attention units to model the internal correlation between high-level and low-level features. Patil et al. [29] develop an optimized architecture that adopts a Siamese-based pre-trained encoder with an attention-based UNet decoder to reconstruct fine-grained feature maps. Lv et al. [30] combine spatial-spectral attention mechanism and multi-scale dilation convolution modules to capture changes that have a greater degree of positivity.

The structure of the attention mechanism places a limitation, in that the features can only be enhanced on a specific scale (channel, spatial, or positional), while ignoring the sequential relationships between the two streams. Thus, inspired by MHN, we introduce the deeply supervised feature retrieval module into the change detection framework.

### B. Image Retrieval and Feature Aggregation

The content-based image retrieval aims to search for relevant images, given query image, from a large-scale database by analyzing the color, texture, or shape of the contents [31]. The exponential growth of visual data has promoted the rapid development of this scenario in the field of computer vision and multimedia. Generally speaking, content-based image retrieval, which comprises instance and semantic tasks [32], requires the accurate and efficient retrieval of discriminative feature representations over a large-scale image collection.

With the development of feature extractors over the past two decades, image retrieval has undergone astonishing progress with the development of feature extractors. Before the breakthrough of deep learning, handcrafted features such as Bag of visual Words (BoW) [33] and SIFT [34] were most

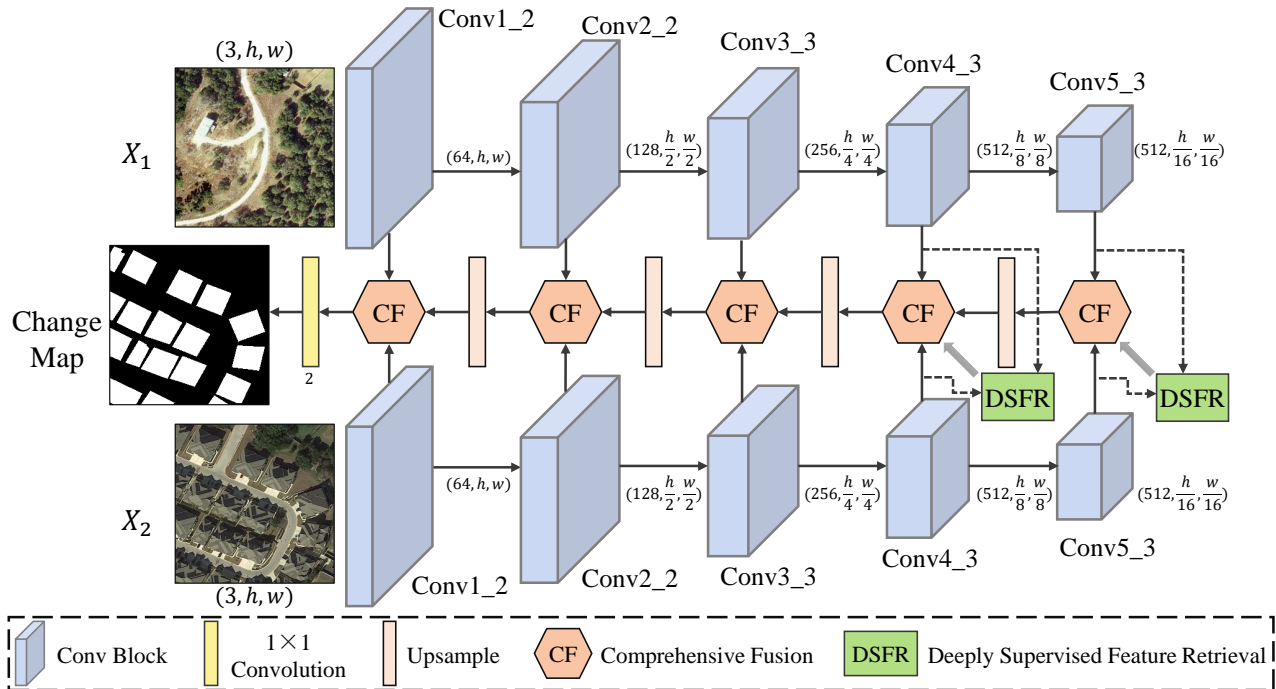


Fig. 3. The overall architecture of the Dsfer-Net. The feature extractor is a Siamese architecture with shared weights. VGG-16 before pool5 is utilized as the backbone. DSFR modules are used for feature aggregation and retrieval in deep layers. CF blocks comprehensively fuse the multi-scale features.

frequently used. Then, deep learning, which can effectively learn multi-level feature representations directly from data, emerged, yielding irrefutably superior performance in this field. As is known, the structure details of features produced by convolutional layers are connected only to the local region of the image with a certain receptive field. To further promote the discriminability of activation extracted from deep CNNs and help retrieve specific instances, feature embedding and aggregation strategies have been introduced to image retrieval. In [35], Noh et al. present an attentive local feature descriptor to select keypoint features based on convolutional neural networks for large-scale landmark retrieval. Chaudhuri et al. propose a Siamese graph convolutional network that uses contrastive loss to minimize the most discriminative embedding space for remote sensing image retrieval [36]. Other aggregation metrics have been combined with off-the-shelf deep learning models for image retrieval, such as Vector of Locally Aggregated Descriptors (VLAD) [37], Selective Match Kernel (SMK) [38], deep hashing embedding [39], among others.

In contrast to previously mentioned image retrieval systems, in this work, we propose a deeply supervised feature retrieval module that can accomplish the retrieval process in the deep convolutional layers directly. It should be noted that this module retrieves the deep differential features under supervision using a modern Hopfield network and aggregates retrieved feature pairs, which will be passed forward for bitemporal remote sensing change detection.

### C. Modern Hopfield Networks

Hopfield Networks, introduced in the 1980s in [40], [41], are energy-based binary neural networks that are associative

memories, i.e. were designed to store and retrieve binary valued data. Building on work in [42]–[48] proposing polynomial terms in the energy function, [49] demonstrated that using exponential terms the storage capacity of these classical binary Hopfield networks can be considerably increased. Here, in contrast to these binary associative memory networks, we use modern Hopfield networks as introduced in [50], [51] which work on continuous inputs, i.e. can store and retrieve real valued data. Crucially, unlike their classical counterparts, these modern Hopfield networks (MHNs) are differentiable and can thus be trained by gradient descent. They also retain the key ability of their binary counterparts to store exponentially many samples that can be retrieved in only one update step. Successful applications of MHNs include solving large-scale multi-instance learning tasks [52], predicting few- and zero-shot chemical reaction templates [53] and conducting hierarchical prototype learning and improving text-image embedding representations for remote sensing image generation tasks [54].

In this paper, following our previous study [55] where we retrieved reliable and explainable deep features using MHN, we propose a deeply supervised feature retrieval module that adopts the Hopfield layer for bitemporal change detection to better understand and exploit the real changes between the sequential images, while we further explore appropriate applications of the prototype Hopfield layer for semantic segmentation.

## III. METHODOLOGY

### A. Overview

The overall architecture of the proposed Dsfer-Net is shown in Fig. 3. The paired images are input to a Siamese convolutional neural network to extract multi-level deep features. The

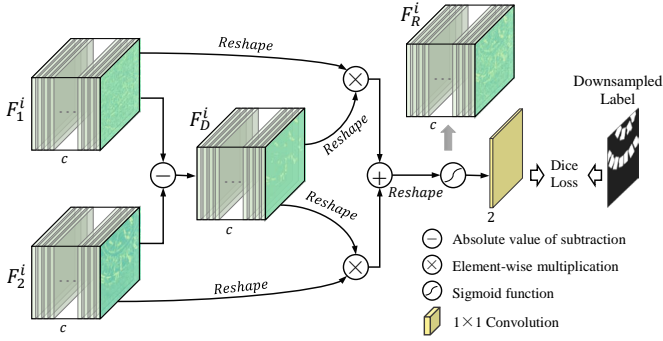


Fig. 4. Deeply supervised feature retrieval (DSFR) module.  $(F_1^i, F_2^i)$  represents the  $i$ -th paired feature maps extracted by the feature extractor. For the proposed network, the DSFR module is conducted on the fourth and fifth feature pairs, where  $i = 4, 5$ .

encoder is built based on VGG-16 with pre-trained parameters whose final fully-connected layers and last pooling layer are removed. To decode the extracted multi-scale feature maps, we propose the comprehension fusion (CF) strategy and design deeply supervised feature retrieval (DSFR) modules. To capture semantic and sequential information from the deep layers, two DSFR modules are applied to aggregate and retrieve the feature difference in the hidden layers, and the multi-scale features from convolutional layers (Conv1\_2, Conv2\_2, Conv3\_3, Conv4\_3, Conv5\_3) are hierarchically integrated with retrieved features by the proposed CF strategy.

Let  $X_1 \in \mathbb{R}^{3 \times h \times w}$  and  $X_2 \in \mathbb{R}^{3 \times h \times w}$  denote the paired images captured from different times ( $t_1$  and  $t_2$ ), respectively, and  $Y$  represents the annotated change map, where  $h$  and  $w$  represent the height and weight of the image, respectively. The main steps of this binary change detection task can be briefly described as follows:

- 1) First, the image pair is fed into the feature extractor with shared weights, through which five pairs of multi-scale raw feature maps  $\{(F_1^i, F_2^i)\}_{i=1}^5$  are obtained.
- 2) For higher-level features, i.e.,  $i = 4, 5$ , the DSFR module is applied to obtain an intermediate change map that maintains the change of interests. The dice loss is calculated based on the change map and the downsampled label.
- 3) In the meantime, feature maps of two streams are concatenated and decoded by the CF strategy, and the change map  $F_R^i$  retrieved from dual Hopfield layers of the DSFR module are forwarded, as the weight mask of concatenated features. Then the multi-scale features are merged and decoded in the same dimension, and the cross entropy loss is calculated based on the fused feature map and the ground-truth label.
- 4) Finally, the whole network is minimized by a combination of cross entropy loss and the dice losses using backpropagation.

### B. Deeply Supervised Feature Retrieval

For the extracted deep feature maps, our intuition is that the changes between the feature pairs should also be preserved and traceable. However, the high-level features are usually

too abstract and semantic to maintain the important texture information related to the change of interests, as has been previously shown in Fig. 2.

To exploit the semantic gaps between the bitemporal image features and aggregate sequential information, we propose a deeply supervised feature retrieval (DSFR) module for the deepest features. The structure of the DSFR module, which is mainly constructed by dual Hopfield layers, is shown in Fig. 4. Given a deep feature pair  $(F_1^i, F_2^i)$ , the DSFR module calculates the absolute value of the difference feature, reshapes the features, and retrieves the difference feature through a Hopfield-type layer that treats the two respective deep features as the stored patterns. Then, the retrieved features are merged and normalized as a deep change map.

The prototype of the Hopfield layer, originally proposed in [50], can learn or retrieve the state pattern in deep neural networks with multi-type structures and changeable application fields. To better fit MHNs to the proposed binary change detection task, the difference feature is defined as the state pattern to help activate the memory nodes that are highly associated with changing information stored in the raw features. Before passing to the Hopfield layer, the given features are first reshaped into 2-D matrices in which  $F_D^i \in \mathbb{R}^{(h'w') \times c}$  denotes the 2-D absolute difference feature and the raw feature  $F_j^i \in \mathbb{R}^{(h'w') \times c}$ ,  $j = 1, 2$  denotes the store pattern, where  $c$ ,  $h'$ , and  $w'$  are the depth, height, and weight of the feature, respectively. For each Hopfield layer, the output of the retrieved difference feature is expressed as:

$$F_{R_j}^i = \text{softmax}(\beta F_D^i W_D W_S^T F_j^{i\top}) F_j^i W_S, \quad (1)$$

where  $\text{softmax}(\cdot)$  denotes the row-wise softmax function, and  $\beta$  is a scaling parameter.  $W_D$  and  $W_S$  are learnable parameters that project the state pattern and store pattern, respectively, into a unified space. To further enhance the efficacy of the dual Hopfield layers, the retrieved features are merged and normalized as one change map:

$$F_R^i = \sigma(F_{R_1}^i + F_{R_2}^i), \quad (2)$$

where  $\sigma$  denotes a sigmoid function.

The role of DSFR module has two aspects: 1) the retrieved deep change map directly flows forward to the CF block as a weight mask to highlight changed regions of the features extracted from shallower layers; and 2) the retrieved deep change map is fed into a  $1 \times 1$  convolutional layer to generate an intermediate change map  $M_i \in \mathbb{R}^{2 \times h' \times w'}$ , and the dice loss is calculated according to the intermediate change map and the downsampled label.

### C. Comprehensive Fusion

To fuse feature maps, the most straightforward process is to concatenate the two stream features and the feature from deeper layers directly into one feature map. However, a direct combination of the heterogeneous features inevitably increases the training difficulties. To incorporate the deep change map retrieved from the DSFR module into the raw feature maps and fuse multi-scale features in an efficient way, a comprehensive fusion strategy is designed and implemented as so called CF

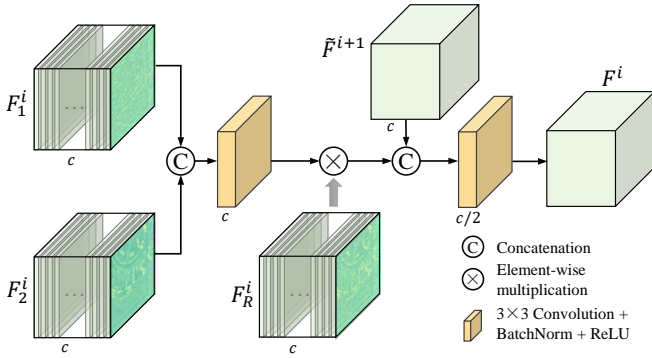


Fig. 5. Comprehensive Fusion (CF) strategy.  $(F_1^i, F_2^i)$  represents the  $i$ -th paired feature maps extracted by the feature extractor. If  $i = 4, 5$ , the concatenate features are multiplied with the retrieved feature  $F_R^i$ .  $\tilde{F}^{i+1}$  represents the upsampled feature obtained from the deeper CF block.

blocks. A detailed illustration of the CF strategy is shown in Fig. 5. Given a raw feature pair  $(F_1^i, F_2^i)$ , the CF block first concatenates these two features and feeds them into a  $3 \times 3$  convolutional layer. For the deepest layers, i.e.,  $i = 4$  and  $5$ , the retrieved change map  $F_R^i$  is input as a mask of the concatenated features. The multiplied feature emphasizes the changed information and suppresses the unchanged regions. The multiplied feature then concatenates the upsampled CF feature  $\tilde{F}^{i+1}$  from deeper layers and decodes the concatenated feature through another  $3 \times 3$  convolutional layer as the output map of the  $i$ -th CF block of the whole network. Formally, the CF feature map of the  $i$ -th stage can be expressed as

$$F^i = f_2^{(3 \times 3)}(\text{Concat}(f_1^{(3 \times 3)}(\mathcal{F}^i) \odot F_R^i, \tilde{F}^{i+1})), \quad (3)$$

where each  $f^{(3 \times 3)}(\cdot)$  denotes a convolution layer with kernel size  $3 \times 3$  and the appropriate number of channels linked to  $i$  as shown in Fig. 5, followed by a batch normalization layer (BN) and a ReLU activation layer,  $\text{Concat}(\cdot, \cdot)$  denotes the concatenation of two features,  $\mathcal{F}^i = \text{Concat}(F_1^i, F_2^i)$  represents the concatenated feature of  $F_1^i$  and  $F_2^i$ , and  $\odot$  denotes element-wise multiplication.

#### D. Network Training

It has been proved that the binary cross-entropy loss function performs effectively for two-class problems by treating the softmax layer as a pixel-wise classification problem [56]. However, for typical change detection datasets, the class distribution of changed and unchanged pixels is usually heavily imbalanced. To relieve this class-imbalance problem, we adopt the weighted binary cross-entropy loss function to train our model. This function can be expressed as follows

$$\mathcal{L}_{wbce} = -\frac{1}{hw} \sum_{l=1}^{hw} (w_1 Y_l \log \hat{Y}_l + w_0 (1 - Y_l) \log (1 - \hat{Y}_l)), \quad (4)$$

where  $w_0$  and  $w_1$  represent the weight for the unchanged class and the changed class, respectively, and  $Y_l$  and  $\hat{Y}_l$  denote the  $l$ -th pixel of the annotated change map and the predicted change map, respectively.

In the DSFR module, the dice loss is also calculated for deeper convolutional features. Let  $i$  denote the  $i$ -th basic stage of the backbone network; thus, the downsampled annotated change map and the intermediate predicted change map can be respectively represented as  $Y^i$  and  $\hat{Y}^i$ , and the dice loss can be written as

$$\mathcal{L}_{dice}^i = 1 - 2 \cdot \frac{\sum_{m=1}^{h'w'} Y_m^i \hat{Y}_m^i}{\sum_{m=1}^{h'w'} (Y_m^i + \hat{Y}_m^i)}, \quad (5)$$

where  $Y_m^i$  and  $\hat{Y}_m^i$  denote the  $m$ -th pixel of the downsampled label and the intermediate prediction, respectively. In this study, we can derive the relationships of the heights and weights between the original annotated change map and the intermediate map are

$$\begin{aligned} h' &= 2^{1-i} \cdot h, \\ w' &= 2^{1-i} \cdot w. \end{aligned} \quad (6)$$

Finally, the objective function for training the proposed network can be formulated as:

$$\mathcal{L}_{total} = \mathcal{L}_{wbce} + \lambda \cdot (\mathcal{L}_{dice}^4 + \mathcal{L}_{dice}^5)/2, \quad (7)$$

where  $\lambda$  is the weighting factor to adjust respective loss terms.

## IV. EXPERIMENTS AND DISCUSSION

In this study, the proposed Dsfer-Net is conducted on three widely used CD datasets and compared with seven state-of-the-art algorithms. Detailed implementation and evaluation metrics are illustrated bellow. Finally, the experimental results are provided and discussed in detail.

### A. Dataset Description and Evaluation Metrics

We carried out the experiments on three CD datasets:

1) **LEVIR-CD** is a large-scale building change detection dataset that covers 20 different regions in Texas, US. It contains 637 very high-resolution (VHR) Google Earth (GE) image patch pairs with a size of  $1024 \times 1024$  pixels and a spatial resolution of 0.5 m/pixel. Following [57], we divided the image pairs into training, validation, and test datasets with an approximate ratio of 7:1:2. The original images were cropped into 16 small patches of sizes of  $256 \times 256$ . Thus, there is a total of 7,120 image pairs for training, 1,024 for validation, and 2,048 for testing.

2) **WHU-CD** is a subset of the WHU Building dataset [58] which contains both aerial and satellite imagery. The building change subset covers an area of 20.5 km<sup>2</sup> in Christchurch, New Zealand where a 6.3-magnitude earthquake occurred in February 2011 and was rebuilt in the following years. One image pair with a size of  $32,507 \times 15,354$  pixels and a spatial resolution of 0.075 m/pixel was collected in 2012 and 2016, respectively. To conduct the experiments, we cropped the original images into 8189 non-overlapped tiles with  $256 \times 256$  pixels and split the cropped tiles into a training set, a validation set, and a test set with a ratio of 6:1:3. Thus, there is a total of 4,572 image pairs for training, 762 for validation, and 2,286 for testing.

3) **CDD** [59] is a season-varying remote sensing dataset collected from Google Earth (DigitalGlobe) that consists of seven pairs of manually ground-truth created season-varying images with  $4725 \times 2700$  pixels and four pairs of season-varying images with minimal changes and resolution of  $1900 \times 1000$  pixels. The spatial resolution of the images is  $0.03 \sim 1$  m/pixel. By cropping the original images with a size of  $256 \times 256$  and a randomly rotated fragment ( $0 \sim 2\pi$ ), 16,000 pairs were obtained, with 10,000 and 3,000 pairs used for training and validation, respectively, and the remaining 3,000 pairs were used for testing.

To quantitatively evaluate the performance of the proposed method, precision (P), recall (R), F1-score, overall accuracy (OA), and Intersection over Union (IoU) were chosen as the evaluation metrics, which are defined as follows:

$$P = \frac{TP}{TP + FP}$$

$$R = \frac{TP}{TP + FN}$$

$$F1 = \frac{2PR}{P + R}$$

$$OA = \frac{TP + TN}{TP + FP + TN + FN}$$

$$IoU = \frac{TP}{TP + FP + FN}$$

where TP, TN, FP, and FN represent the number of true positives, true negatives, false positives, and false negatives, respectively.

### B. Comparative Methods and Implementation Settings

To validate the performance of our model, we compared the proposed Dsfer-Net with seven state-of-the-art approaches. A brief introduction to the comparative methods follows.

- FC-Siam-conc [25] is a U-Net-based architecture that applies a Siamese encoding stream in order to extract deep features from both images separately; then it concatenates the extracted features with two skip connections and passes them to the decoding stream.
- FC-Siam-diff [25] has the same feature extractor as FC-Siam-conc. However, the absolute value of feature differences is concatenated with the deep feature in the decoding stream, instead of concatenating both features together.
- FC-EF-Res [27] is an early fusion architecture that first concatenates the bitemporal images together and passes them through the network. Unlike traditional convolutional layers, residual blocks have been added to improve network performance and facilitate training.
- STANet [57] designs a self-attention mechanism to model the spatial-temporal relationships of the bitemporal images and capture the dependencies at various scales. The attentive weights between the features are then calculated to generate more discriminative features.
- BiT [60] is a transformer-based module that uses visual words to express the space-time changes from high-level concepts. The Bitemporal image Transformer (BiT) is

incorporated in a deep feature differencing-based network for change detection.

- DSAMNet [61] employs two deeply supervised layers to assist the learning of the hidden layer and designs a metric module to stack the resized features of different scales. Convolutional block attention modules (CBAMs) are adopted to make the features more discriminative.
- FrNet [55] is a preliminary study that utilizes the MHNs to integrate deep features. The Hopfield pooling layer [50], [51] is utilized together with the deepest convolutional layer, and the VGG-16 is selected as the feature extractor.

All the experiments were implemented on Pytorch and trained using NVIDIA A100 GPU. To compare the efficiency of the comparative methods fairly, we consider both the parametric settings specified in the original literature and the actual performance, and report the best performance. For the proposed Dsfer-Net, we set the projection dimension of the Hopfield layers to 512. We adopt the Adam optimizer with an initial learning rate of  $5e-5$  on the LEVIR-CD and the WHU-CD dataset, and that of  $1e-4$  on the CDD dataset. The learning rate will linearly decay to 0 after 30,000 iterations. We set the weight decay to  $1e-5$  and the batch size to 32. Validation is performed after every 500 iterations, and the best model on the validation set is used for evaluation on the test set. The same training, validation, and testing settings are adopted on all three datasets.

### C. Benchmark Comparison and Analysis

In this section, the proposed model is compared with seven state-of-the-art methods on three benchmark datasets. The visualized results are shown in Fig. 6, where the TP, FP, TN, and FN are shown in white, cyan, black, and red, respectively. In the LEVIR-CD and WHU-CD datasets, buildings are the changed objects to be evaluated. It can be observed that most of the methods can correctly detect small buildings in both the LEVIR-CD and WHU-CD datasets. However, FC-Siam-conc and FC-Siam-diff failed to distinguish the unchanged land-covers surrounding the buildings, resulting in a high incidence false alarms compared to other methods. This indicates that directly concatenating the deep features or the feature differences can not effectively provide discriminative information for network training. For large-size buildings, the STANet, BiT, and DSAMNet cannot correctly detect the objects, especially for those buildings that have rather complex shapes. The results show that although the well-received attention mechanism is capable of re-integrating and emphasizing interesting information about deep features, its application determines that it suffers from a self-retrieval mechanism and may fail to highlight real differences between the temporal images. Compared to FrNet, the proposed model can better control the false alarms and provide clearer boundaries between the changed objects. Among all the methods, our method performs the best in detecting the changed objects and returns the most accurate contours of the buildings. We conclude that the designed DSFR module is helpful in extracting real changes from time-series data and preserving details as close to the ground-truth as possible.

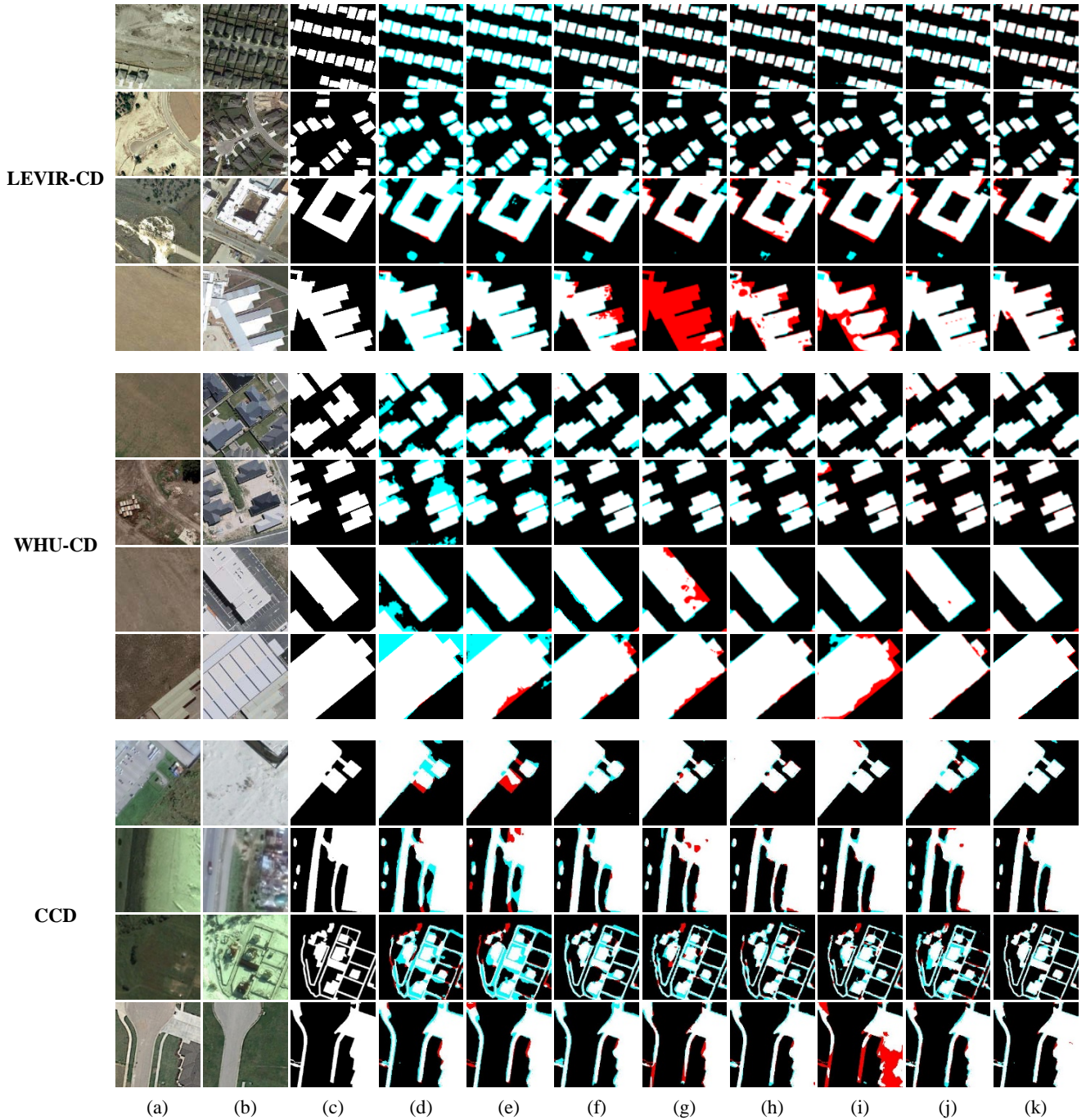


Fig. 6. Visualization examples of different methods on the LEVIR-CD, WHU-CD, and CDD datasets. (a) Image from  $t_1$ . (b) Image from  $t_2$ . (c) Ground-truth. (d) FC-Siam-conc. (e) FC-Siam-diff. (f) FC-EF-Res. (g) STANet. (h) BiT. (i) DSAMNet. (j) FrNet. (k) Dsfer-Net. TP, FP, TN, and FN are represented in white, cyan, black, and red, respectively.

The CDD dataset records the seasonal variations and object changes of the ground at different times. It can be seen that the proposed method achieves better results than other comparative methods. As shown in Fig. 6, buildings, roads, and cars are selected as the changed objects for visualization; these changes are caused by time, extreme weather, and human activities. Visualized results show that our model can extract both small-size and large-size changes in the CDD dataset, and have the fewest FP and FN compared to other methods. Even for relatively complex semantic scenes, the proposed

model can accurately detect those real changed objects. In contrast to our model, FC-Siam-conc and FC-Siam-diff can not avoid false alarms when detecting the changes. Furthermore, they perform badly in preserving the boundary of the narrow roads and small objects. Although FC-EF-Res, STANet, BiT, and FrNet can extract changing objects that have relatively large areas, they still have poor performance in detecting fine-grained changes. The DSAMNet, as a deeply supervised and attentive-based method, performs well with respect to identifying narrow and small changes, but suffers from missed

TABLE I  
QUANTITATIVE COMPARISON RESULTS ON THREE DATASETS.

	LEVIR-CD					WHU-CD					CDD				
	P	R	F1	OA	IoU	P	R	F1	OA	IoU	P	R	F1	OA	IoU
FC-Siam-conc	68.29	<b>96.93</b>	80.12	97.55	66.84	64.95	93.57	76.68	97.90	62.18	77.31	88.94	82.72	95.61	70.53
FC-Siam-diff	70.94	96.22	81.67	97.80	69.01	75.23	91.51	82.57	98.57	70.32	81.58	83.81	82.68	95.86	70.47
FC-EF-Res	79.71	93.62	86.11	98.46	75.61	87.92	86.49	87.20	99.06	77.31	85.66	<b>94.85</b>	90.02	97.52	81.86
STANet	86.55	87.99	87.27	98.69	77.41	90.55	83.75	87.02	99.08	77.02	88.92	90.83	89.86	97.58	81.59
BiT	86.30	90.17	88.19	98.77	78.87	89.57	85.72	87.60	99.10	77.94	92.49	91.22	91.85	98.09	84.92
DSAMNet	82.49	90.00	86.08	98.52	75.56	83.49	90.18	86.71	99.05	76.53	91.84	94.14	92.97	98.32	86.87
FrNet	86.80	90.91	88.81	98.83	79.87	<b>93.76</b>	88.72	91.17	99.37	83.77	89.83	91.52	90.67	97.78	82.92
Dsfer-Net	<b>92.15</b>	89.42	<b>90.76</b>	<b>99.04</b>	<b>83.09</b>	91.04	<b>94.17</b>	<b>92.58</b>	<b>99.46</b>	<b>86.18</b>	<b>96.69</b>	93.70	<b>95.17</b>	<b>98.84</b>	<b>90.79</b>

\* Note: All the scores are reported in percentage (%), and the best results are highlighted in **Bold**.

TABLE II  
PERFORMANCE CONTRIBUTION OF DIFFERENT STRATEGIES IN DSFER-NET.

	CF DSFR	LEVIR-CD	WHU-CD	CDD
BaseNet+Concat		89.97	91.87	93.91
BaseNet+CF	✓	90.05	91.88	94.70
BaseNet+CF+DSFR	✓ ✓	<b>90.76</b>	<b>92.58</b>	<b>95.17</b>

\* Note: All the scores are reported in percentage (%), and the best F1 scores are highlighted in **Bold**.

detection for large-size objects and fails to retain the internal compactness of objects.

The quantitative evaluations of all the methods are illustrated in Table I. Given that our method is proposed for binary change detection, we only focus on reporting the accuracy of the changed class. In all three datasets, the proposed model has the best results in F1 score, OA, and IoU. In the LEVIR-CD dataset, the F1 score and IoU of Dsfer-Net exceed the best performed comparative methods by 1.9 and 3.2 points, respectively. In the WHU-CD dataset, our model outperforms FrNet by 1.4 point of F1 score and 2.4 point point of IoU. And in the CDD dataset, the proposed method achieves a 2.2 point higher F1 score and a 3.9 point higher IoU than DSAMNet. Additionally, we find that the precision and recall of the methods are often negatively correlated, which can be intuitively understood because false alarms and miss detection usually do not occur simultaneously; thus, change detection methods needs to compromise between detecting more positives and controlling false alarms. In the quantitative comparisons of various datasets, the proposed method shows the best performance, with fewer false alarms and reasonable missed detection.

#### D. Ablation Study

To verify the efficacy of our designed CF strategy and the DSFR modules, ablation studies are conducted on three datasets: BaseNet+Concat, BaseNet+CF, and BaseNet+CF+DSFR. As the name suggests, BaseNet+Concat is a Siamese network with VGG-16 as the backbone; it uses the concatenated feature as the input of the decoder. The BaseNet+CF adopts the CF strategy to integrate multi-scale features, and the BaseNet+CF+DSFR is equivalent to the proposed Dsfer-Net. The F1 scores of different structures are

TABLE III  
SENSITIVITY ANALYSIS OF WEIGHTING FACTOR ON LOSS FUNCTION.

$\lambda$	LEVIR-CD		WHU-CD		CDD	
	F1	OA	F1	OA	F1	OA
0.001	90.69	99.04	92.58	99.46	95.01	98.80
0.01	90.73	99.04	<b>92.58</b>	<b>99.46</b>	94.83	98.75
0.1	<b>90.76</b>	<b>99.04</b>	92.56	99.46	94.99	98.79
1	90.66	99.03	92.34	99.45	<b>95.17</b>	<b>98.84</b>
10	90.12	98.96	92.04	99.43	94.75	98.75
100	89.47	98.88	92.75	99.48	94.49	98.68

\* Note: All the scores are reported in percentage (%), and the best results are highlighted in **Bold**.

illustrated in Table II. It can be found that compared to the classic feature concatenation process, the CF strategy brings slight improvements in the three datasets. It is also found that combining the CF strategy and the DSFR model can benefit the change detection performance more than that of the feature concatenations. It should be noted that although the BaseNet+Concat is constructed only by a feature extractor and convolutional layers, it still outperforms other ResNet-based networks, such as STANet, BiT, and DSAMNet, which suggests that adopting appropriate structures to extract multi-scale features will also affect the performance of the network.

#### E. Sensitivity Analysis

As described in Section III, the loss function of the proposed network is constructed by the cross entropy loss and the dice losses balanced by a weighting factor. To explore the influence of different values on training the proposed network, comparative experiments are conducted on three datasets by setting different  $\lambda$  values. Since the DSFR modules are adopted to improve feature extraction capability and to preserve the texture information in the deep layers, the best value of  $\lambda$  represents the most appropriate proportion of the retrieval features for the training process. Note that when  $\lambda$  is set to 0, the network is equivalent to the second baseline “BaseNet+CF” in the previous subsection. As can be seen in Table III, a relatively smaller value of  $\lambda$  is more beneficial to the performance. It is known that the shape of the changed objects will slightly change and the texture information of the details will also be lost after repeated downsampling. Adding appropriate weights to the deep supervision modules can help

capture the location of the changed objects over the scenes, but higher weights may cause false alarms on fine-grained landcovers and result in poorer performances. Specifically, for the LEVIR-CD, WHU-CD, and CDD datasets, the best performance is obtained when the values of  $\lambda$  equal to 0.1, 0.01, and 1, respectively.

### F. Visualizations of the Hopfield Features

To further evaluate the effect of the DSFR modules, we give a visualization of the retrieved features in three datasets. The DSFR module is mainly constructed by a dual Hopfield layer and is implemented on the fourth and fifth convolutional stages; thus, the aggregated Hopfield features are compared with the downsampled image pairs, and the labels in the same size.

As shown in Figs. 7–9, there are obvious differences between the image pairs after downsampling in all three datasets, such as the color, illuminations, and even some of the unchanged objects. But the deeply supervised feature retrieval module strengthens the ability to capture texture structures in deep layers by emphasizing the consistency between the intermediate change maps and the downsampled labels, thus making the network more robust to real changes. In the LEVIR-CD and CDD datasets, it can be observed that the change of interests is highlighted effectively through the DSFR modules in the deeper layers, and the intermediate change maps are consistent with the downsampled ground-truths. In the CDD dataset, small objects such as narrow roads and cars can also be retrieved effectively by the dual Hopfield layers. For the WHU-CD dataset, it can be seen from Fig. 8 that the difference feature retrieved in the fourth stage is not so accurate. This is mainly because the WHU dataset records the target area before and after the earthquake. During this period, rapid post-disaster reconstruction and urban expansion took place, resulting in tremendous changes in new buildings, roads, squares, and vegetations. Therefore, the retrieved difference features are very different from the building change labels. On the other hand, it can be found that as the network goes deeper, the DSFR module can locate the change information more accurately in the fifth stage.

## V. CONCLUSION

In this paper, we propose a deep supervision and feature retrieval network for change detection in remote sensing images. Inspired by the modern Hopfield network, we retrieve the difference features and aggregate the sequential information in a deeply supervised manner. To concatenate multi-level features reasonably, the comprehensive fusion strategy is adopted into the decoder. Extensive experiments have been conducted on three widely used change detection datasets to validate the effectiveness of the proposed method. In the two building change detection datasets, the proposed model can better preserve the contour of the buildings by avoiding false alarms for dense buildings and controlling miss detection for irregular and independent buildings. For the seasonal variation dataset, the proposed model can accurately capture the real changes among pseudo seasonal variations and detect small

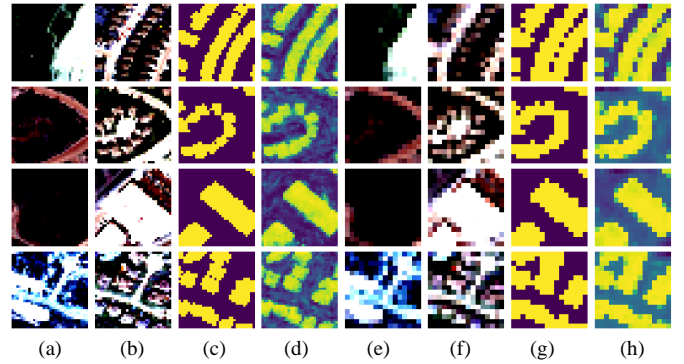


Fig. 7. Visualization examples of deep features retrieved by DSFR modules in the LEVIR-CD dataset. (a) Images from  $t_1$  downsampled by 8. (b) Images from  $t_2$  downsampled by 8. (c) Ground-truths downsampled by 8. (d) Retrieved features from the fourth stage. (e) Images from  $t_1$  downsampled by 16. (f) Images from  $t_2$  downsampled by 16. (g) Ground-truths downsampled by 16. (h) Retrieved features from the fifth stage.

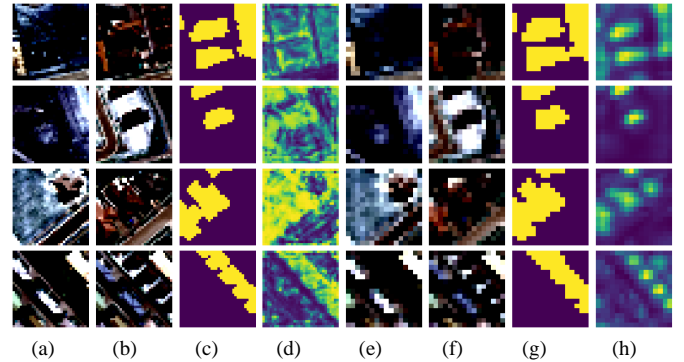


Fig. 8. Visualization examples of deep features retrieved by DSFR modules in the WHU-CD dataset. (a) Images from  $t_1$  downsampled by 8. (b) Images from  $t_2$  downsampled by 8. (c) Ground-truths downsampled by 8. (d) Retrieved features from the fourth stage. (e) Images from  $t_1$  downsampled by 16. (f) Images from  $t_2$  downsampled by 16. (g) Ground-truths downsampled by 16. (h) Retrieved features from the fifth stage.

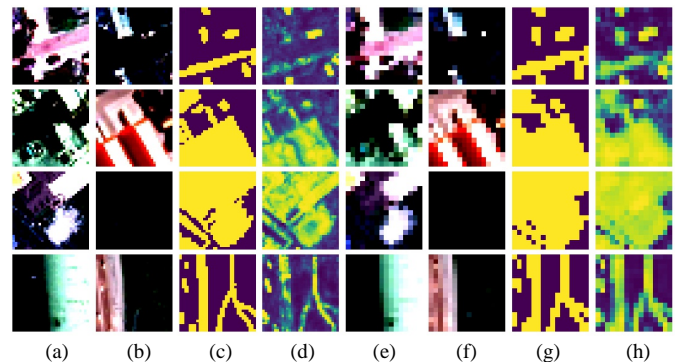


Fig. 9. Visualization examples of deep features retrieved by DSFR modules in the CDD dataset. (a) Images from  $t_1$  downsampled by 8. (b) Images from  $t_2$  downsampled by 8. (c) Ground-truths downsampled by 8. (d) Retrieved features from the fourth stage. (e) Images from  $t_1$  downsampled by 16. (f) Images from  $t_2$  downsampled by 16. (g) Ground-truths downsampled by 16. (h) Retrieved features from the fifth stage.

and narrow objects as well. Through an ablation study and sensitivity analysis, we verified the promotion effect of the DSFR model on the backbone network and identified reasonable parametric settings. Finally, visualization examples show the performance of the Hopfield layer on difference feature retrieval and aggregation. Through experiments, we found that the feature retrieval module might fail to locate the change of interests accurately in deeper layers when many unexpected changes occur in the scene. Therefore, we will continue to work on designing appropriate structures to overcome the side effects of pseudo-changes. In addition, in our future work, we hope to extend this study to off-nadir and semantic change detection tasks.

#### ACKNOWLEDGMENTS

The authors would like to thank the authors of all comparative methods for sharing their codes, the contributors of the LEVIR-CD, WHU-CD, and CDD datasets, Dr. Yonghao Xu for his valuable comments and discussions, and the Institute of Advanced Research in Artificial Intelligence (IARAI) for its support.

#### REFERENCES

- [1] H. Jiang, M. Peng, Y. Zhong, H. Xie, Z. Hao, J. Lin, X. Ma, and X. Hu, "A survey on deep learning-based change detection from high-resolution remote sensing images," *Remote Sensing*, vol. 14, no. 7, p. 1552, 2022.
- [2] J. Prendes, M. Chabert, F. Pascal, A. Giros, and J.-Y. Tourneret, "A new multivariate statistical model for change detection in images acquired by homogeneous and heterogeneous sensors," *IEEE Transactions on Image Processing*, vol. 24, no. 3, pp. 799–812, 2014.
- [3] Z. Zheng, Y. Zhong, J. Wang, A. Ma, and L. Zhang, "Building damage assessment for rapid disaster response with a deep object-based semantic change detection framework: From natural disasters to man-made disasters," *Remote Sensing of Environment*, vol. 265, p. 112636, 2021.
- [4] M. J. Carlotto, "Detection and analysis of change in remotely sensed imagery with application to wide area surveillance," *IEEE Transactions on Image Processing*, vol. 6, no. 1, pp. 189–202, 1997.
- [5] B. Desclée, P. Bogaert, and P. Defourny, "Forest change detection by statistical object-based method," *Remote Sensing of Environment*, vol. 102, no. 1–2, pp. 1–11, 2006.
- [6] R. Touati, M. Mignotte, and M. Dahmane, "Multimodal change detection in remote sensing images using an unsupervised pixel pairwise-based markov random field model," *IEEE Transactions on Image Processing*, vol. 29, pp. 757–767, 2019.
- [7] L. Ru, B. Du, and C. Wu, "Multi-temporal scene classification and scene change detection with correlation based fusion," *IEEE Transactions on Image Processing*, vol. 30, pp. 1382–1394, 2020.
- [8] E. F. Lambin and A. H. Strahlers, "Change-vector analysis in multitemporal space: A tool to detect and categorize land-cover change processes using high temporal-resolution satellite data," *Remote Sensing of Environment*, vol. 48, no. 2, pp. 231–244, 1994.
- [9] B. Du, L. Ru, C. Wu, and L. Zhang, "Unsupervised deep slow feature analysis for change detection in multi-temporal remote sensing images," *IEEE Transactions on Geoscience and Remote Sensing*, vol. 57, no. 12, pp. 9976–9992, 2019.
- [10] Z. Liu, G. Li, G. Mercier, Y. He, and Q. Pan, "Change detection in heterogenous remote sensing images via homogeneous pixel transformation," *IEEE Transactions on Image Processing*, vol. 27, no. 4, pp. 1822–1834, 2017.
- [11] C. Zhang, P. Yue, D. Tapete, L. Jiang, B. Shangguan, L. Huang, and G. Liu, "A deeply supervised image fusion network for change detection in high resolution bi-temporal remote sensing images," *ISPRS Journal of Photogrammetry and Remote Sensing*, vol. 166, pp. 183–200, 2020.
- [12] X. Peng, R. Zhong, Z. Li, and Q. Li, "Optical remote sensing image change detection based on attention mechanism and image difference," *IEEE Transactions on Geoscience and Remote Sensing*, vol. 59, no. 9, pp. 7296–7307, 2020.
- [13] Q. Li, R. Zhong, X. Du, and Y. Du, "TransUNetCD: A hybrid transformer network for change detection in optical remote-sensing images," *IEEE Transactions on Geoscience and Remote Sensing*, vol. 60, pp. 1–19, 2022.
- [14] Y. Lei, X. Liu, J. Shi, C. Lei, and J. Wang, "Multiscale superpixel segmentation with deep features for change detection," *IEEE Access*, vol. 7, pp. 36 600–36 616, 2019.
- [15] J. Yosinski, J. Clune, A. Nguyen, T. Fuchs, and H. Lipson, "Understanding neural networks through deep visualization," *arXiv preprint arXiv:1506.06579*, 2015.
- [16] B. Hou, Q. Liu, H. Wang, and Y. Wang, "From W-Net to CDGAN: Bitemporal change detection via deep learning techniques," *IEEE Transactions on Geoscience and Remote Sensing*, vol. 58, no. 3, pp. 1790–1802, 2019.
- [17] S. Sun, L. Mu, L. Wang, and P. Liu, "L-UNet: An LSTM network for remote sensing image change detection," *IEEE Geoscience and Remote Sensing Letters*, 2020.
- [18] Y. Zhou, F. Wang, J. Zhao, R. Yao, S. Chen, and H. Ma, "Spatial-temporal based multi-head self-attention for remote sensing image change detection," *IEEE Transactions on Circuits and Systems for Video Technology*, 2022.
- [19] Y. Sun, L. Lei, D. Guan, and G. Kuang, "Iterative robust graph for unsupervised change detection of heterogeneous remote sensing images," *IEEE Transactions on Image Processing*, vol. 30, pp. 6277–6291, 2021.
- [20] H. Zhang, M. Gong, P. Zhang, L. Su, and J. Shi, "Feature-level change detection using deep representation and feature change analysis for multispectral imagery," *IEEE Geoscience and Remote Sensing Letters*, vol. 13, no. 11, pp. 1666–1670, 2016.
- [21] J. Chen, Z. Yuan, J. Peng, L. Chen, H. Huang, J. Zhu, Y. Liu, and H. Li, "DASNet: Dual attentive fully convolutional siamese networks for change detection in high-resolution satellite images," *IEEE Journal of Selected Topics in Applied Earth Observations and Remote Sensing*, vol. 14, pp. 1194–1206, 2020.
- [22] S. Ji, Y. Shen, M. Lu, and Y. Zhang, "Building instance change detection from large-scale aerial images using convolutional neural networks and simulated samples," *Remote Sensing*, vol. 11, no. 11, p. 1343, 2019.
- [23] H. Zhang, M. Lin, G. Yang, and L. Zhang, "Escnet: An end-to-end superpixel-enhanced change detection network for very-high-resolution remote sensing images," *IEEE Transactions on Neural Networks and Learning Systems*, 2021.
- [24] T. Liu, L. Yang, and D. Lunga, "Change detection using deep learning approach with object-based image analysis," *Remote Sensing of Environment*, vol. 256, p. 112308, 2021.
- [25] R. C. Daudt, B. Le Saux, and A. Boulch, "Fully convolutional siamese networks for change detection," in *2018 25th IEEE International Conference on Image Processing (ICIP)*. IEEE, 2018, pp. 4063–4067.
- [26] Y. Chen, X. Ouyang, and G. Agam, "Mfcnet: End-to-end approach for change detection in images," in *2018 25th IEEE International Conference on Image Processing (ICIP)*. IEEE, 2018, pp. 4008–4012.
- [27] R. C. Daudt, B. Le Saux, A. Boulch, and Y. Gousseau, "Multitask learning for large-scale semantic change detection," *Computer Vision and Image Understanding*, vol. 187, p. 102783, 2019.
- [28] D. Peng, Y. Zhang, and H. Guan, "End-to-end change detection for high resolution satellite images using improved UNet++," *Remote Sensing*, vol. 11, no. 11, p. 1382, 2019.
- [29] P. S. Patil, R. S. Holambe, and L. M. Waghmare, "EffCDNet: Transfer learning with deep attention network for change detection in high spatial resolution satellite images," *Digital Signal Processing*, vol. 118, p. 103250, 2021.
- [30] Z. Lv, F. Wang, G. Cui, J. A. Benediktsson, T. Lei, and W. Sun, "Spatial-spectral attention network guided with change magnitude image for land cover change detection using remote sensing images," *IEEE Transactions on Geoscience and Remote Sensing*, vol. 60, pp. 1–12, 2022.
- [31] W. Chen, Y. Liu, W. Wang, E. Bakker, T. Georgiou, P. Fieguth, L. Liu, and M. S. Lew, "Deep learning for instance retrieval: A survey," *arXiv preprint arXiv:2101.11282*, 2021.
- [32] B. Barz and J. Denzler, "Content-based image retrieval and the semantic gap in the deep learning era," in *International Conference on Pattern Recognition*. Springer, 2021, pp. 245–260.
- [33] J. Sivic and A. Zisserman, "Video google: A text retrieval approach to object matching in videos," in *IEEE International Conference on Computer Vision*, vol. 3. IEEE Computer Society, 2003, pp. 1470–1470.

- [34] D. G. Lowe, "Distinctive image features from scale-invariant keypoints," *International Journal of Computer Vision*, vol. 60, no. 2, pp. 91–110, 2004.
- [35] H. Noh, A. Araujo, J. Sim, T. Weyand, and B. Han, "Large-scale image retrieval with attentive deep local features," in *Proceedings of the IEEE International Conference on Computer Vision*, 2017, pp. 3456–3465.
- [36] U. Chaudhuri, B. Banerjee, and A. Bhattacharya, "Siamese graph convolutional network for content based remote sensing image retrieval," *Computer Vision and Image Understanding*, vol. 184, pp. 22–30, 2019.
- [37] Y. Gong, L. Wang, R. Guo, and S. Lazebnik, "Multi-scale orderless pooling of deep convolutional activation features," in *European Conference on Computer Vision*. Springer, 2014, pp. 392–407.
- [38] J. Yang, J. Liang, H. Shen, K. Wang, P. L. Rosin, and M.-H. Yang, "Dynamic match kernel with deep convolutional features for image retrieval," *IEEE Transactions on Image Processing*, vol. 27, no. 11, pp. 5288–5302, 2018.
- [39] T.-T. Do, D.-K. Le Tan, T. T. Pham, and N.-M. Cheung, "Simultaneous feature aggregating and hashing for large-scale image search," in *Proceedings of the IEEE Conference on Computer Vision and Pattern Recognition*, 2017, pp. 6618–6627.
- [40] J. J. Hopfield, "Neural networks and physical systems with emergent collective computational abilities," *Proceedings of the National Academy of Sciences*, vol. 79, no. 8, pp. 2554–2558, 1982.
- [41] —, "Neurons with graded response have collective computational properties like those of two-state neurons," *Proceedings of the national academy of sciences*, vol. 81, no. 10, pp. 3088–3092, 1984.
- [42] H. H. Chen, Y. C. Lee, G. Z. Sun, H. Y. Lee, T. Maxwell, and C. L. Giles, "High order correlation model for associative memory," *AIP Conference Proceedings*, vol. 151, no. 1, pp. 86–99, 1986.
- [43] D. Psaltis and H. P. Cheol, "Nonlinear discriminant functions and associative memories," *AIP Conference Proceedings*, vol. 151, no. 1, pp. 370–375, 1986.
- [44] P. Baldi and S. S. Venkatesh, "Number of stable points for spin-glasses and neural networks of higher orders," *Phys. Rev. Lett.*, vol. 58, pp. 913–916, 1987.
- [45] E. Gardner, "Multiconnected neural network models," *Journal of Physics A*, vol. 20, no. 11, pp. 3453–3464, 1987.
- [46] L. F. Abbott and Y. Arian, "Storage capacity of generalized networks," *Phys. Rev. A*, vol. 36, pp. 5091–5094, 1987.
- [47] D. Horn and M. Usher, "Capacities of multiconnected memory models," *J. Phys. France*, vol. 49, no. 3, pp. 389–395, 1988.
- [48] D. Krotov and J. J. Hopfield, "Dense associative memory for pattern recognition," *Advances in Neural Information Processing Systems*, vol. 29, 2016.
- [49] M. Demircigil, J. Heusel, M. Löwe, S. Uppgang, and F. Vermet, "On a model of associative memory with huge storage capacity," *Journal of Statistical Physics*, vol. 168, no. 2, pp. 288–299, 2017.
- [50] H. Ramsauer, B. Schäfl, J. Lehner, P. Seidl, M. Widrich, L. Gruber, M. Holzleitner, M. Pavlović, G. K. Sandve, V. Greiff, D. Kreil, M. Kopp, G. Klambauer, J. Brandstetter, and S. Hochreiter, "Hopfield networks is all you need," *ArXiv*, vol. 2008.02217, 2020.
- [51] —, "Hopfield networks is all you need," in *Proc. Int. Conf. Learn. Representations*, 2021.
- [52] M. Widrich, B. Schäfl, M. Pavlović, H. Ramsauer, L. Gruber, M. Holzleitner, J. Brandstetter, G. K. Sandve, V. Greiff, S. Hochreiter *et al.*, "Modern hopfield networks and attention for immune repertoire classification," *Advances in Neural Information Processing Systems*, vol. 33, pp. 18 832–18 845, 2020.
- [53] P. Seidl, P. Renz, N. Dyubankova, P. Neves, J. Verhoeven, M. Segler, J. K. Wegner, S. Hochreiter, and G. Klambauer, "Modern hopfield networks for few-and zero-shot reaction template prediction," *arXiv preprint arXiv:2104.03279*, 2021.
- [54] Y. Xu, W. Yu, P. Ghamisi, M. Kopp, and S. Hochreiter, "Txt2Img-MHN: Remote sensing image generation from text using modern hopfield networks," *arXiv preprint arXiv:2208.04441*, 2022.
- [55] S. Chang, M. Kopp, and P. Ghamisi, "A deep feature retrieved network for bitemporal remote sensing image change detection," 2022.
- [56] Y. Lei, D. Peng, P. Zhang, Q. Ke, and H. Li, "Hierarchical paired channel fusion network for street scene change detection," *IEEE Transactions on Image Processing*, vol. 30, pp. 55–67, 2020.
- [57] H. Chen and Z. Shi, "A spatial-temporal attention-based method and a new dataset for remote sensing image change detection," *Remote Sensing*, vol. 12, no. 10, p. 1662, 2020.
- [58] S. Ji, S. Wei, and M. Lu, "Fully convolutional networks for multisource building extraction from an open aerial and satellite imagery data set," *IEEE Transactions on Geoscience and Remote Sensing*, vol. 57, no. 1, pp. 574–586, 2018.
- [59] M. Lebedev, Y. V. Vizilter, O. Vygolov, V. Knyaz, and A. Y. Rubis, "Change detection in remote sensing images using conditional adversarial networks," *International Archives of the Photogrammetry, Remote Sensing & Spatial Information Sciences*, vol. 42, no. 2, 2018.
- [60] H. Chen, Z. Qi, and Z. Shi, "Remote sensing image change detection with transformers," *IEEE Transactions on Geoscience and Remote Sensing*, vol. 60, pp. 1–14, 2021.
- [61] Q. Shi, M. Liu, S. Li, X. Liu, F. Wang, and L. Zhang, "A deeply supervised attention metric-based network and an open aerial image dataset for remote sensing change detection," *IEEE Transactions on Geoscience and Remote Sensing*, vol. 60, pp. 1–16, 2021.